Ab Initio Molecular Dynamics Study of Methanol Adsorption on Copper Clusters

Wen-Dung Hsu,[†] Masahiko Ichihashi,[‡] Tamotsu Kondow,[‡] and Susan B. Sinnott*[,†]

Department of Materials Science and Engineering, University of Florida, Gainesville, Florida, 32611-6400, and Cluster Research Laboratory, Toyota Technological Institute, 717-86 Futamata Ichikawa, Chiba 272-0001, Japan

Received: August 31, 2006; In Final Form: November 1, 2006

The preferential structures of small copper clusters Cu_n ($n = 2-9$) and the adsorption of methanol molecules on these clusters are examined with first principles, molecular dynamics simulations. The results show that the copper clusters undergo systematic changes in bond length and bond order associated with altering their preferential structures from one-dimensional structures, to two-dimensional and three-dimensional structures. The results also indicate that low coordination number sites on the copper clusters are both the most favorable for methanol adsorption and have the greatest localization of electronic charge. The simulations predict that charge transfer between the neutral copper clusters and the incident methanol molecules is a key process by which adsorption is stabilized. Importantly, the changes in the dimensionality of the copper clusters do not significantly influence methanol adsorption.

Introduction

Methanol is predicted to be an important component in the next generation of renewable green fuels, and there has recently been interest in the use of methanol in fuel cells.[1] It is produced using transition metal catalysts, so there is considerable interest in better understanding the reactivity of surface intermediates during methanol synthesis[3−15] to improve the efficiency of surface reactions and the heterogeneous catalysis process as a whole.

Atomic clusters effectively connect the atomic scale to the macroscopic scale of bulk crystals and provide an excellent platform from which one can study the heterogeneous catalysis process on various surface structures. Experimentally, there has been tremendous progress in recent years in the production and study of clusters.[16−20] There have also been numerous computational studies[21−26] that have provided insight into the structure, stability, and reactivity of clusters that is complementary to the experimental data.

The interaction of methanol molecules with metal clusters changes with the size (number of the constituent atoms) of the cluster and has been shown to be quite different from their interaction with metal surfaces. For instance, experiments find that methanol molecules undergo chemisorption primarily with clusters that consist of six atoms, demethanation occurs mainly with clusters that consist of four atoms, and carbide formation occurs with clusters that consist of seven to eight atoms for nickel cluster ions.[27] In contrast, in the case of copper cluster ions, chemisorption occurs at clusters that consist of four atoms with a gradual increase above this size, demethanation occurs at clusters that consist of six atoms, and HOH formation occurs on clusters that consist of four to five atoms.[28] Note that not only the reaction cross-section but also the reaction itself changes dramatically with the size of the cluster. In contrast, physisorption dominates on metal surfaces.[11,29]

The dissociation energy of a bare copper cluster is found to oscillate as the size of the cluster increases.[21,22] This oscillation behavior is also found in many other metal clusters.[30,31] In general, clusters with "magic" number sizes have high dissociation energies and are considered to be stable. In a typical metal cluster such as an alkali metal cluster (in a liquid-like state), this oscillatory behavior can be explained by the jellium model.[32,33] In this model, the delocalized valence electrons of the metal cluster interact with a uniform background built by the positive core ions to form a spheroidal potential well. This leads to discrete electronic levels (shells) with angular momenta L and degeneracy $2L + 1$.[34] According to the energy levels of these shells, the clusters with completely filled shells are more stable and harder to dissociate than those with partially filled shells. Although the jellium model provides good insight into the characteristics of metal clusters, its application is limited to qualitative discussion. For instance, in a theoretical study of the reaction of a methanol molecule on a copper cluster, both the properties of the cluster and the molecule need to be considered on the basis of a more sophisticated theoretical methodology.

Experiments on the collision of a methanol molecule with a metal cluster yield the reaction products, from which one may infer possible reaction paths. However, it is possible to directly determine only the mass of the products and not their structures from these experiments. In this regard, theoretical calculations are helpful in understanding the details of the reactions. Typically, the electronic structures of various rigid isomers are calculated to determine local minima on the potential energy surface. These theoretical results may then be compared with the experimental data to determine which cluster isomers actually emerge in the real reactions.[35] An adduct, i.e., an adsorbed methanol molecule on a metal cluster, can be studied by similar methods. Of course, the behavior of the adduct is diverse, and there are many questions that need to be solved, such as how does the molecule adsorb (adsorption site and geometry), what is the nature of the bonding between the

* To whom correspondence should be addressed. E-mail: ssinn@mse.ufl.edu.
[†] University of Florida.
[‡] Toyota Technological Institute.

10.1021/jp065669s CCC: $37.00
Published on Web 12/23/2006

molecule and the metal cluster, do the properties of the adsorbed molecule change as the cluster grows, and so forth.

In this work, the properties of copper clusters (Cu_n, $n = 2-9$) are determined from density functional theory (DFT) calculations. Different approximation methods for exchange and correlation, and both spin-polarized and non-spin-polarized wave functions are used. The results are compared with experimental data to verify the validity of the methods. Methanol molecules are then deposited on the copper clusters in DFT molecular dynamics simulations (DFT−MD), and the final equilibrium adsorption structures are analyzed. The results provide insight into how methanol molecules adsorb on copper clusters.

Computational Details

Because the reactions of interest involve transition metals reacting chemically with organic molecules, most empirical or semiempirical methods are not optimal approaches for this study due to their lack of predictive accuracy for systems with heterogeneous bonding characteristics. Therefore, DFT calculations are used, which have been shown to be good at modeling the components of the current system.[26,36−38] In addition, the DFT−MD approach is used to model the methanol molecular interactions with the clusters. In particular, the Born−Oppenheimer MD approach[39,40] is used, in which Newton's equations of motion are solved to determine ionic motion followed by self-consistent determining of the electronic structure.

The calculations and simulations are carried out using the CAmbridge Serial Total Energy Package (CASTEP) software, a first principle simulation code developed by Payne and coworkers.[41,42] The DFT calculations and DFT−MD simulations make use of (1) a plane-wave basis to represent the wavefunctions, (2) pseudopotentials[43] that replace the ionic cores, and (3) the use of fast Fourier transforms (FFT's). The exchange-correlation energy is described by the local density approximation (LDA) or the generalized gradient approximation (GGA).[44] Ionic cores are described by ultrasoft pseudopotentials,[43] and the valence electrons are described with plane waves that have a kinetic energy cutoff of 270 eV.

The calculations include two parts. The first part involves the optimization of the Cu_n clusters, where $n = 2-9$. In these optimization calculations, both non-spin-polarized and spin-polarized wave functions are used to compare the effect of spin-polarization on the results. The size of the supercell used in this calculation is 10 Å × 10 Å × 10 Å. The second part involves modeling the collisions of the methanol molecules with the clusters. Specifically, the methanol molecules have external kinetic energies of 0.5 eV/molecule and are incident on the Cu clusters in each collision. In the case of the collisions, the supercell is increased to 15 Å in the direction of molecular motion toward the Cu cluster. The initial distance between a copper cluster and a methanol molecule is around 3−4 Å. The NVT ensemble[45−48] is used to maintain the system temperature at 300 K, and the time step in the DFT−MD simulations is 1 fs. Each trajectory runs for between 1 and 6 ps, with the end of the simulation depending on the outcome of the molecule−cluster collision. The potential energy drops when the outcome is adsorption of the methanol to the copper. The total energy convergence is tested with respect to system supercells as large as 20 Å × 20 Å × 20 Å, *k*-point meshes up to 3 × 3 × 3, and kinetic energy cutoff up to 320 eV. The results indicate that the differences in Cu cluster absolute total energy are about 0.2 eV/atom with the conditions that are used in this study relative to the most computationally expensive conditions, while the differences in copper cluster binding energies are about 0.01 eV/atom.

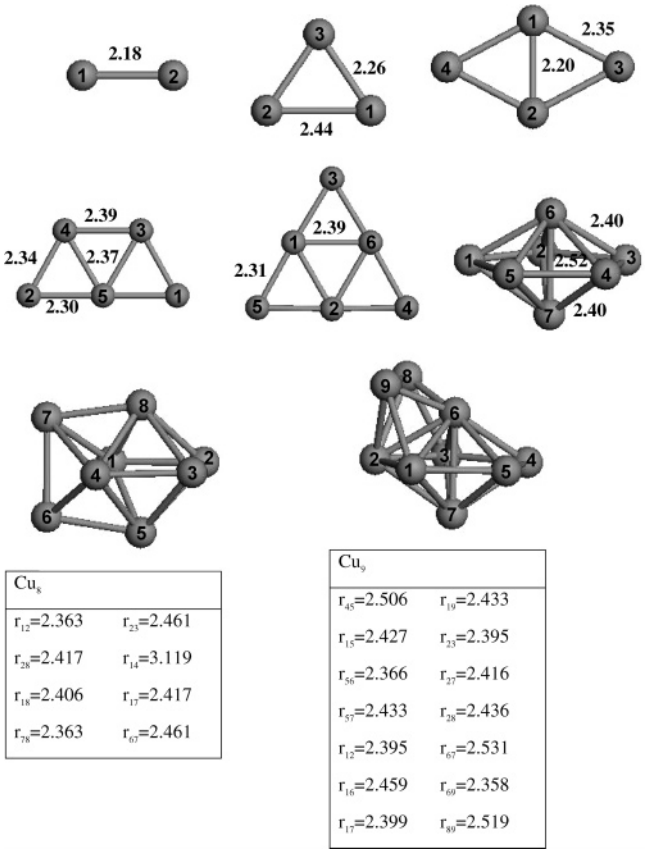

Cu_8	
r_{12}=2.363	r_{23}=2.461
r_{28}=2.417	r_{14}=3.119
r_{18}=2.406	r_{17}=2.417
r_{78}=2.363	r_{67}=2.461

Cu_9	
r_{45}=2.506	r_{19}=2.433
r_{15}=2.427	r_{23}=2.395
r_{56}=2.366	r_{27}=2.416
r_{57}=2.433	r_{28}=2.436
r_{12}=2.395	r_{67}=2.531
r_{16}=2.459	r_{69}=2.358
r_{17}=2.399	r_{89}=2.519

Figure 1. Ground-state structures of the neutral copper clusters after optimization using the generalized gradient approximation (GGA) and nonpolarized wave function in the calculations.

Results and Discussion

I. Structure of Neutral Copper Clusters. The ground-state structure of neutral copper clusters has been investigated by Jug et al.[22] and Jaque and Torro-Labbe,[21] and the ground-state structures of the clusters examined in this study are constructed on the basis of these published findings. The structures of these neutral copper clusters are then optimized within the DFT calculations using either the LDA or the GGA. The final geometries obtained by optimization with the GGA and non-polarized wave functions are shown in Figure 1. As the cluster size increases, the structure of the cluster changes from a linear configuration that is one-dimensional (Cu_2) to planar structures that are two-dimensional (Cu_3-Cu_6), and finally to fully three-dimensional structures (Cu_7-Cu_9). In addition, Table 1 provides detailed bond lengths optimized by the LDA and compares the details of the optimized structures to published results. Examination of the data indicates that the average bond lengths predicted in these calculations are around 5% smaller than those obtained using the LDA method with Gaussian-type basis sets,[22] and around 9% smaller than those obtained using the B3LPY method with Gaussian-type basis sets.[21]

Figure 2 illustrates the average bond length versus copper cluster size as optimized using either the LDA or GGA with and without the inclusion of spin polarization, and Table 2 provides the relevant structural details. The results show that the average Cu−Cu bond length increases when the cluster size increases and its dimensionality changes. For example Cu_2 has the shortest bond length and is a one-dimensional (linear)

TABLE 1: Comparison of Ground-State Structure of Neutral Copper Clusters, Cu_n ($n = 2-9$)

Cu clusters	PG	this work (LDA plane-wave-type basis set)		Jug et al. (LDA Gaussian-type basis set)[22]		Jaque and Toro-Labbe (B3PW91 Gaussian-type basis set)[21]	
Cu_2	D_h	$r_{12} = 2.142$		$r_{12} = 2.21$		$r_{12} = 2.254$	
Cu_3	C_{2v}	$r_{12} = 2.246$	$r_{13} = 2.257$	$r_{12} = 2.50$	$r_{13} = 2.26$	$r_{12} = 2.690$	$r_{13} = 2.326$
Cu_4	D_{2h}	$r_{12} = 2.195$	$r_{13} = 2.282$	$r_{12} = 2.24$	$r_{13} = 2.36$	$r_{12} = 2.574$	$_{13} = 2.293$
Cu_5	C_{2v}	$r_{25} = 2.243$	$r_{45} = 2.300$	$r_{25} = 2.32$	$r_{45} = 2.36$	$r_{25} = 2.401$	$r_{45} = 2.451$
		$r_{24} = 2.264$	$r_{34} = 2.289$	$r_{24} = 2.33$	$r_{34} = 2.38$	$r_{24} = 2.415$	$r_{34} = 2.469$
Cu_6	D_{3h}	$r_{15} = 2.250$	$r_{16} = 2.316$	$r_{34} = 2.33$	$r_{45} = 2.39$	$r_{34} = 2.404$	$r_{45} = 2.484$
Cu_7	D_{5h}	$r_{34} = 2.329$	$r_{36} = 2.335$	$r_{34} = 2.39$	$r_{36} = 2.39$	$r_{34} = 2.500$	$r_{36} = 2.500$
Cu_8	C_{2v}	$r_{12} = 2.302$	$r_{23} = 2.379$	$r_{12} = 2.35$	$r_{23} = 2.47$	$r_{12} = 2.437$	$r_{23} = 2.643$
		$r_{28} = 2.330$	$r_{14} = 3.022$	$r_{28} = 2.38$	$r_{14} = 3.07$	$r_{28} = 2.491$	$r_{14} = 3.225$
		$r_{18} = 2.347$	$r_{17} = 2.333$	$r_{18} = 2.39$	$r_{17} = 2.38$	$r_{18} = 2.512$	$r_{17} = 2.491$
		$r_{78} = 2.300$	$r_{67} = 2.379$	$r_{78} = 2.35$	$r_{67} = 2.47$	$r_{78} = 2.436$	$r_{67} = 2.643$
Cu_9	C_s	$r_{45} = 2.426$	$r_{19} = 2.353$	$r_{45} = 2.49$	$r_{19} = 2.42$	$r_{45} = 2.615$	$r_{19} = 2.521$
		$r_{15} = 2.350$	$r_{23} = 2.344$	$r_{15} = 2.39$	$r_{23} = 2.39$	$r_{15} = 2.521$	$r_{23} = 2.650$
		$r_{56} = 2.309$	$r_{27} = 2.360$	$r_{56} = 2.35$	$r_{27} = 2.40$	$r_{56} = 2.463$	$r_{27} = 2.479$
		$r_{57} = 2.347$	$r_{28} = 2.341$	$r_{57} = 2.42$	$r_{28} = 2.42$	$r_{57} = 2.555$	$r_{28} = 2.559$
		$r_{12} = 2.342$	$r_{67} = 2.483$	$r_{12} = 2.39$	$r_{67} =$	$r_{12} = 2.500$	$r_{67} = 2.650$
		$r_{16} = 2.401$	$r_{69} = 2.310$	$r_{16} = 2.46$	$r_{69} = 2.35$	$r_{16} = 2.555$	$r_{69} = 2.463$
		$r_{17} = 2.341$	$r_{89} = 2.426$	$r_{17} = 2.40$	$r_{89} =$	$r_{17} = 2.500$	$r_{89} = 2.614$

TABLE 2: Average Bond Length $\langle r_{Cu}-Cu \rangle$ in angstroms and Mean Coordination Number (CN) of Cu_n Clusters

Cu clusters	LDA	LDA + spin	GGA	GGA + spin	Jug et al.[22]	Jaque and Toro-Labbe[21]	CN
Cu_2	2.142	2.142	2.180	2.180	2.210	2.254	1.0
Cu_3	2.246	2.245	2.326	2.332	2.340	2.447	2.0
Cu_4	2.264	2.264	2.328	2.328	2.336	2.418	2.5
Cu_5	2.272	2.271	2.348	2.341	2.343	2.429	2.8
Cu_6	2.272	2.273	2.338	2.338	2.350	2.431	3.0
Cu_7	2.341	2.343	2.413	2.412	2.390	2.500	4.3
Cu_8	2.333	2.334	2.407	2.404	2.386	2.501	4.5
Cu_9	2.364	2.364	2.430	2.431	2.453	2.534	5.1

structure. Cu_3–Cu_6 have intermediate bond lengths and are two-dimensional (planar) structures. At cluster sizes of seven and greater, three-dimensional clusters are preferred that have the largest Cu−Cu bond lengths. This evolution of the cluster structure occurs as a result of the influence of the hybridization of 3d, 4s, and 4p orbitals.[49] In particular, the hybridization of the 3d and 4p orbitals produces the three-dimensional cluster structures.[50] Because these interactions occur over relatively long distances, they result in larger average bond lengths in the clusters. Table 2 also shows the coordination number (CN) of the copper atoms in the various clusters. The CN increases as the cluster size increases in a manner that is illustrative of the changes in the dimensionality of the cluster. One-dimensional clusters have a CN = 1, two-dimensional clusters have a CN between 2 and 3, and three-dimensional clusters have a CN larger than 4.3.

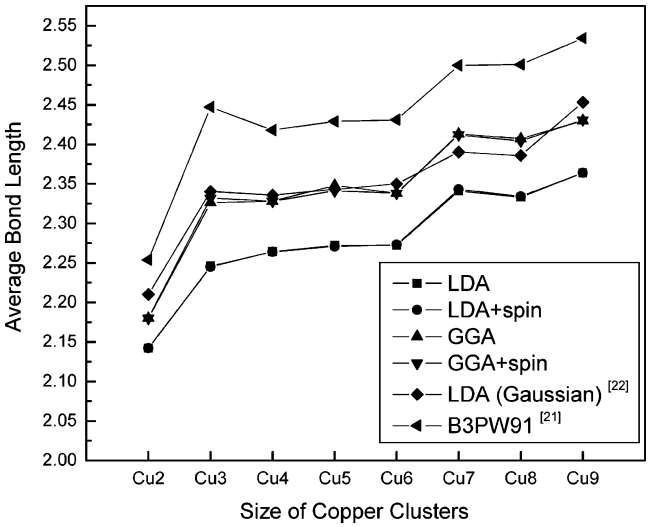

Figure 2. Average Cu−Cu bond lengths in the clusters obtained from the calculations as a function of the level of theory used.

Comparing the results obtained with different exchange-correlation approximation methods, we find that the LDA predicts smaller copper clusters than the GGA. This is not surprising as it is generally accepted that the GGA predicts longer bond lengths than the LDA.[51] Figure 2 also indicates that plane-wave-type basis sets predict smaller cluster sizes than Gaussian-type basis sets. However, the average bond length difference between plane-wave-type basis sets with the LDA and Gaussian-type basis sets with the same approximation[22] differ by no more than 3.5%. This proves that using the LDA and plane-wave basis sets is adequate for the study of the copper clusters. Additionally, Figure 2 indicates that the effect of spin polarization is negligible for the optimization of the structure of the copper clusters.

Figure 3 shows the binding energy as a function of the cluster size. Here, the binding energy is calculated as

$$\mathrm{BE} = (nE_{\mathrm{Cu}} - E_{\mathrm{Cu_n}})/n \qquad (1)$$

where n is the number of atoms in the cluster, E_{Cu} is the energy of a Cu atom in vacuum, and $E_{\mathrm{Cu_n}}$ is the energy of the Cu cluster containing n copper atoms. The errors associated with self-interaction energies in DFT are large in cases of high localization of electron density, such as occur here in the case of the Cu clusters. These errors are minimized here by the fact that comparable levels of electron localization are present in both the initial and final adiabatic states. A similar approach has been successfully used in several comparable studies, such as the catalytic CO oxidation on Au clusters,[52] the interaction of thiolates with Au and Cu clusters,[2] and the interaction of S atoms with Au clusters.[30] Figure 3 illustrates how the binding energy increases monotonically with increasing cluster size. This indicates that it is energetically favorable for the copper atoms

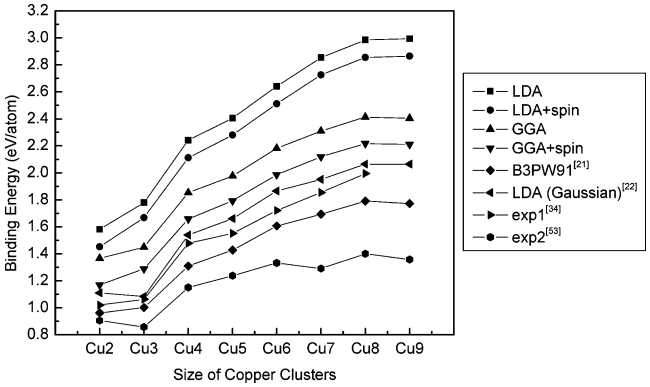

Figure 3. Binding energies in the copper clusters obtained from the calculations as a function of the level of theory used and from experimental data.

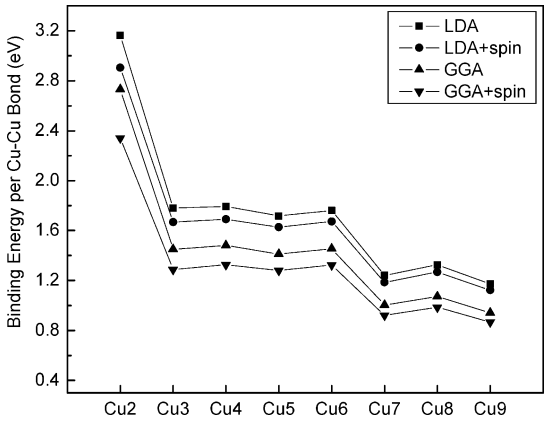

Figure 4. Binding energies per Cu−Cu bond in the clusters as a function of the level of theory used in the calculations.

to form ever larger clusters. Figure 3 also provides a comparison of the binding energy calculated in this and other studies.[21,22,34,53] The larger binding energy (around 38% larger than literature values)[21] that is predicted here is due to the use of the ultrasoft pseudopotential. Calculations that used a cutoff energy of 600 eV with norm-conserving pseudoupotentials, which is indicated in CASTEP as being the same level of accuracy as using ultrasoft pseudopotentials with a cutoff energy of 270 eV, were tested, and the resulting bind energies were similar to published literature values[21] to within 3%. However, the norm-conserving pseudopotentials are about five times more computationally expensive than the ultrasoft pseudopotential in the case of Cu_4, and even more expensive for larger clusters. This finding, coupled with the fact that the ultrasoft pseudopotential gives consistently comparable relative binding energies, makes it suitable for use here.

If the binding energy per atom is divided by CN/2, then the binding energy per Cu−Cu bond can be obtained. This result is plotted in Figure 4, where the dimensionality change of clusters as their size increases is clearly indicated. Specifically, the binding energy per Cu−Cu bond decreases as the dimension of the clusters increases. For the case of the Cu_2 one-dimensional cluster, the binding energy per Cu−Cu bond is predicted to be 2.73 eV by the GGA approximation. However, it is only around 1.45 eV for the two-dimensional clusters and approximately 1.00 eV for the three-dimensional clusters.

Figure 4 reveals the effect of spin polarization on the results. When spin-polarized wave functions are used in the DFT calculations, they predict lower Cu−Cu bond binding energies than do the non-spin-polarized wave functions. In Figure 3, it is clear that using the GGA with spin-polarized wave functions

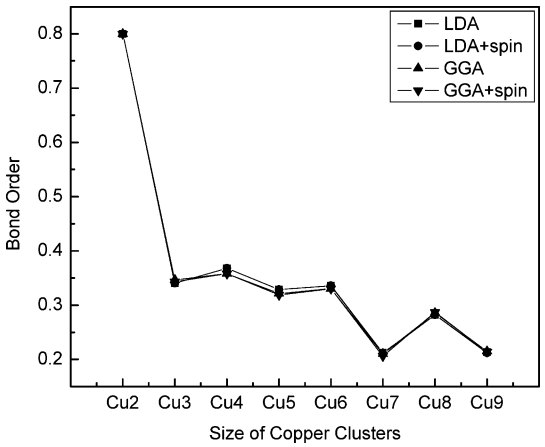

Figure 5. Bond order in the copper clusters as a function of the level of theory used in the calculations.

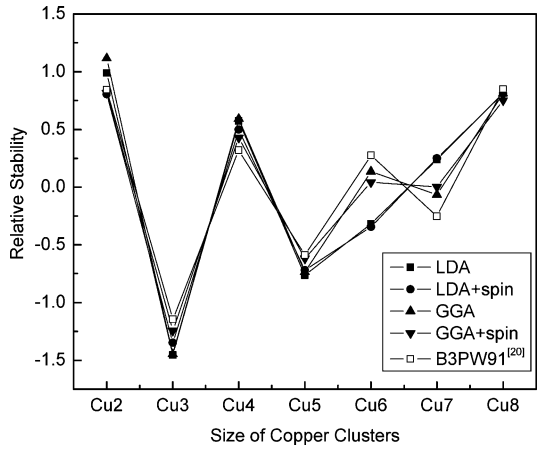

Figure 6. Relative stability of the copper clusters as a function of the approximations used in the calculations.

predicts bond energy results that are in the best agreement with published experimental data.[34,53] It should be mentioned that the experimental data to which the findings are compared are the dissociation energies of anionic and cationic copper clusters rather than the neutral clusters under consideration here.

The average bond order versus cluster size is illustrated in Figure 5. The average bond order is calculated by averaging the Mulliken overlap population[2,54] of the Cu−Cu bonds in the cluster. The bond order value for the Cu_2 cluster is around 0.80, but this drops to around 0.35 for the two-dimensional copper clusters (Cu_3−Cu_6) and to around 0.25 for the three-dimensional copper clusters (Cu_7−Cu_9). The bond order is also indicative of the strength of the bonds within the Cu clusters. Thus the average bond order should be directly proportional to the binding energy per Cu−Cu bond. Comparing Figures 4 and 5, it can be seen that they show similar trends and the ratio between the average bond order and the binding energy per Cu−Cu bond is around 0.5.

Figure 6 indicates the relative stabilities of the different copper clusters. The relative stability is calculated as

$$\Delta_2 E_{Cu_n} = E_{Cu_{n+1}} + E_{Cu_{n-1}} - 2E_{Cu_n} \quad (2)$$

where n is the number of atoms in the cluster. The higher the value of the relative stability, the more stable the cluster. Figure 6 shows that the stability oscillates as a function of cluster size. In particular, the clusters composed of an even number of atoms have higher relative stabilities than those composed of an odd number of atoms. This is because the Cu atom has an electronic

TABLE 3: Atomic Populations for Cu_2-Cu_9 Using the Generalized Gradient Approximation (GGA)

species	ion	$4s^1$	4p	$3d^{10}$	4f	total	charge
Cu_2	1	0.99	0.06	9.95	0.00	11.00	0.00
	2	0.99	0.06	9.95	0.00	11.00	0.00
Cu_3	1	0.94	0.18	9.90	0.00	11.02	-0.02
	2	0.93	0.19	9.90	0.00	11.01	-0.01
	3	0.81	0.24	9.91	0.00	10.97	0.03
Cu_4	1	0.74	0.32	9.90	0.00	10.96	0.04
	2	0.74	0.32	9.90	0.00	10.96	0.04
	3	1.14	0.02	9.87	0.00	11.04	-0.04
	4	1.14	0.02	9.87	0.00	11.04	-0.04
Cu_5	1	1.08	0.04	9.89	0.00	11.02	-0.02
	2	1.08	0.04	9.89	0.00	11.02	-0.02
	3	0.92	0.19	9.88	0.00	10.99	0.01
	4	0.92	0.19	9.88	0.00	10.99	0.01
	5	0.90	0.25	9.84	0.00	10.99	0.01
Cu_6	1	0.90	0.20	9.87	0.00	10.97	0.03
	2	0.89	0.18	9.87	0.00	10.94	0.06
	3	1.15	0.01	9.89	0.00	11.05	-0.05
	4	1.14	0.01	9.89	0.00	11.04	-0.04
	5	1.14	0.01	9.89	0.00	11.04	-0.04
	6	0.90	0.20	9.87	0.00	10.97	0.03
Cu_7	1	0.90	0.29	9.87	0.00	11.06	-0.06
	2	0.90	0.28	9.87	0.00	11.05	-0.05
	3	0.90	0.29	9.87	0.00	11.06	-0.06
	4	0.90	0.28	9.87	0.00	11.05	-0.05
	5	0.90	0.28	9.87	0.00	11.05	-0.05
	6	0.78	0.26	9.83	0.00	10.87	0.13
	7	0.78	0.26	9.83	0.00	10.87	0.13
Cu_8	1	0.82	0.28	9.85	0.00	10.95	0.05
	2	0.91	0.27	9.87	0.00	11.05	-0.05
	3	0.91	0.27	9.87	0.00	11.05	-0.05
	4	0.82	0.28	9.85	0.00	10.95	0.05
	5	0.82	0.28	9.85	0.00	10.95	0.05
	6	0.91	0.27	9.87	0.00	11.05	-0.05
	7	0.91	0.27	9.87	0.00	11.05	-0.05
	8	0.82	0.28	9.85	0.00	10.95	0.05
Cu_9	1	0.81	0.36	9.86	0.00	11.03	-0.03
	2	0.78	0.29	9.84	0.00	10.91	0.09
	3	0.81	0.36	9.86	0.00	11.03	-0.03
	4	0.96	0.24	9.86	0.00	11.05	-0.05
	5	0.96	0.24	9.86	0.00	11.05	-0.05
	6	0.72	0.45	9.79	0.00	10.96	0.04
	7	0.77	0.28	9.84	0.00	10.88	0.12
	8	0.95	0.24	9.86	0.00	11.04	-0.04
	9	0.95	0.24	9.86	0.00	11.04	-0.04

configuration of $[Ar]3d^{10}4s^1$. When an even number of atoms forms a cluster, all the electron orbitals can be fully occupied and form a closed-shell configuration, which stabilizes the cluster relative to the odd-numbered clusters. This finding is in agreement with the predictions of the electronic shell jellium model that says that filled-shell clusters with 2, 8, 18, 20, 40, 58, and 92, etc., valence electrons have increased stability relative to partially filled shell clusters. The numbers of atoms that lead to these valence electron values are the so-called magic numbers.

The relative stabilities obtained using different approximation methods are also compared in Figure 6. Typically, spin-polarized wave functions and non-spin-polarized wavefunctions predict very similar oscillatory behavior; however, the LDA does not predict the oscillatory behavior well when the cluster structure changes from two-dimensional (Cu_6) to three-dimensional (Cu_7). Compared to literature results,[21,22] the GGA is again found to give the most reliable results.

The atomic populations of the copper clusters calculated using the GGA are given in Table 3. As mentioned before, the electronic configuration of a Cu atom is $[Ar]3d^{10}4s^1$. When Cu atoms form the cluster, the 3d and 4s orbitals of each Cu atom became partially occupied. The lost electrons from the 3d and 4s orbitals then occupy the 4p orbital. Thus the interactions between the Cu atoms to form the cluster involve not only 3d and 4s orbitals but also 4p orbitals.

Table 3 also lists the atomic charge on every atom in the cluster. The atomic charge changes on the order of 10^{-2}, but the overall charge on the cluster is zero. It is interesting that the atoms located at the outer cluster sites are more negative, while those at the inner cluster sites are more positive. This indicates that the outer atoms, those farthest from the geometric center of the cluster, have higher electron densities than the inner atoms. The outer atoms also have lower CNs than the inner atoms. For example, in the Cu_3 clusters shown in Figure 1, atoms 1 and 2 are separated by a longer distance than atoms 1 and 3 or atoms 2 and 3. Thus, atoms 1 and 2 are located at the outer sites of the Cu_3 cluster and are consequently negatively charged, while atom 3 is located at the innermost site and is consequently positively charged. Another example is Cu_9, where atoms 2, 6, and 7 are closest to the geometric center of the cluster, at distances of 3.04, 0.19, and 3.08 Å, respectively. In contrast, atoms 1, 3−5, 8, and 9 are farthest away, around 4−6 Å from the geometric center of the cluster. This phenomenon illustrates how the electron clouds in small transition metal clusters are not like those in bulk metals, where the electron density is uniformly distributed.

Table 3 also indicates that among all the copper clusters considered in this study, the negatively charged atoms have larger 4s orbital populations than the positively charged atoms. In the one-dimensional cluster (Cu_2), the two atoms balance each other and are both neutral. In the two-dimensional clusters (Cu_3-Cu_6), the outer atoms have higher 4s orbital populations and have lower 4p orbital populations than the inner site atoms. In the three-dimensional clusters (Cu_7-Cu_9), the outer site atoms have still higher 4s orbital populations than the inner site atoms, but they have almost the same level of 4p orbital population as the inner site atoms. These differences in orbital population are likely responsible for the change in cluster dimensionality that is illustrated in the average bond lengths (Figure 1 and Table 1), binding energy per Cu−Cu bond (Figure 4), and bond order (Figure 5).

II. Collision of Methanol Molecules with Copper Clusters. Figure 7 illustrates the initial and final snapshots from the DFT−MD simulations of the collisions of methanol molecules on the low coordination number sites of the various copper clusters. In all the collisions, the oxygen atom on the methanol molecule adsorbs on the copper clusters, which subsequently distort. The simulations indicate that adsorption occurs when the molecule and cluster are close enough to one another and that their configuration changes immediately following adsorption. The equilibrium structure is determined after their configuration stops changing and a stable bond has been formed. The Cu_4 cluster deforms the most following adsorption of the methanol molecule at the low CN site. In particular, the diamond-shaped structure of the Cu_4 is broken and it transforms to a triangular structure with an extra Cu atom attached to one corner.

Figure 8 illustrates the initial and final snapshots of the collisions of methanol molecules with the high coordination number sites of the copper clusters. In this case, the methanol molecules initially came close to the Cu cluster and then bounced back. The processes repeats several times until the cluster and molecule reach an equilibrium configuration and distance from one another. The equilibrium structure is once again determined after their configuration stops changing and a stable bond has been formed. Again, all the methanol molecules adsorb on the copper cluster through the oxygen atom, and the process distorts the clusters.

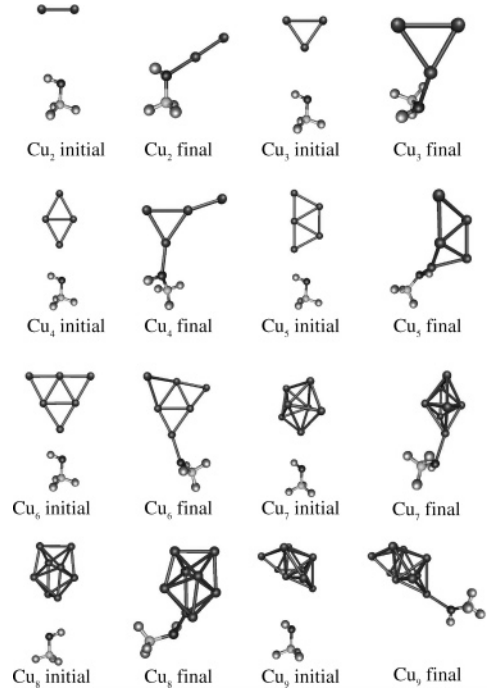

Figure 7. Initial and final snapshots from the simulations of methanol molecule collisions on low coordination number sites of the copper clusters. The oxygen and copper atoms are shown in dark gray, and the carbon and hydrogen are shown in light gray.

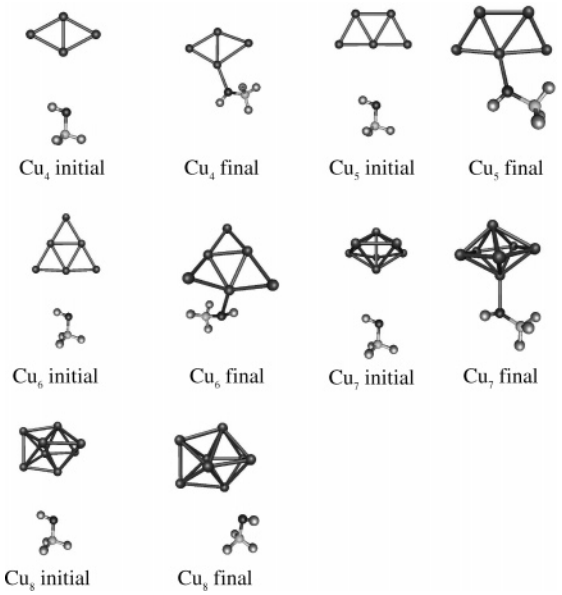

Figure 8. Initial and final snapshots from the simulations of methanol molecule collisions on high coordination sites of the copper clusters. The oxygen and copper atoms are shown in dark gray, and the carbon and hydrogen are shown in light gray.

The simulations indicate that the nearest Cu atom in the cluster to the methanol molecule is attracted to the oxygen atom. This attraction causes the methanol molecule to reorient itself so that the oxygen atom reaches the cluster first. The attraction between the O and Cu atoms make the copper cluster distort toward the methanol molecule. Though the copper cluster distorts in both the collisions on the high CN sites and the low CN sites, the stability of adsorption is different in these two cases. Specifically, molecular adsorption at the low CN site is more stable than at the high CN site. The energy evolution curve indicates that it takes longer for the methanol molecule to stably adsorb to the high CN site of the Cu cluster (because it initially

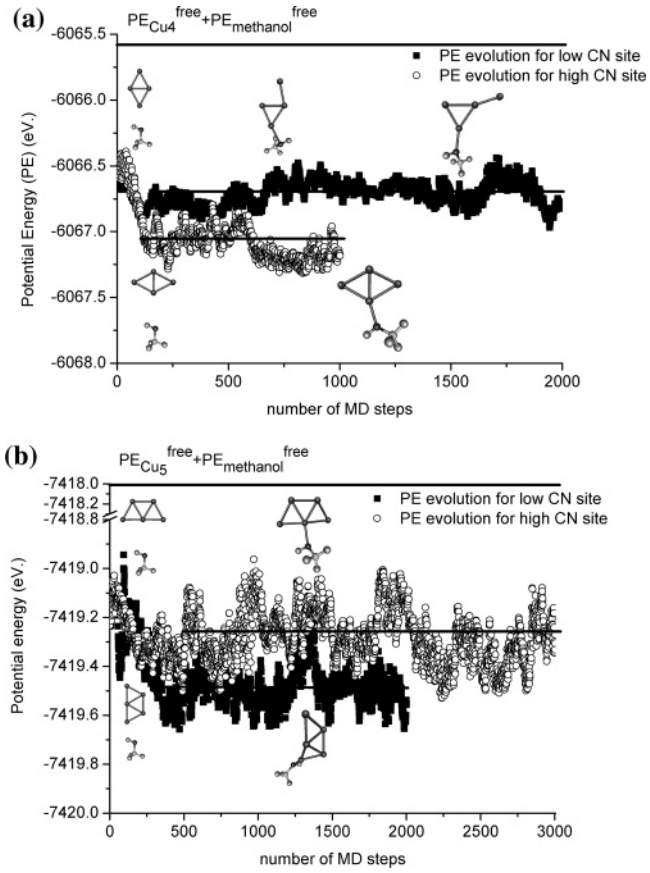

Figure 9. Potential energy evolution of adsorption of methanol on the (a) Cu_4 and (b) Cu_5 clusters. The straight lines indicate the approximate potential energy for methanol adsorbed on the high or low coordination number site of the Cu clusters. The oxygen and copper atoms in the insets are shown in dark gray, and the carbon and hydrogen are shown in light gray.

bounces off the cluster, as described above) than on the low CN site, and there is an obvious energy drop when the methanol molecule adsorbs on the low CN site. Two specific examples for the case of Cu_4 and Cu_5 are given in Figure 9a,b, respectively. In the case of Cu_4, shown in Figure 9a, adsorption on the higher coordination site is more stable than on the lower coordination site, which is the opposite of the other cases considered here. Thus the potential energy curve shows a steep drop as a result of adsorption on the higher coordination site. The Cu_5 case, illustrated in Figure 9b, is more representative of what occurs for the other clusters, where adsorption on the higher coordination site is more stable.

The equilibrium adsorption structure was analyzed by averaging all the equilibrium structures and was characterized in terms of the average Cu−O bond length (Figure 10), the average O−C bond length (Figure 11), the average Cu−O−C bond angle, the average Cu−O−H bond angle, and the average C−O−H bond angle (Figure 12). From these three bond angles, the O solid angle can be characterized by using

$$\Omega_O = 360^o - \theta_{Cu-O-C} - \theta_{Cu-O-H} - \theta_{C-O-H} \qquad (3)$$

where θ_{Cu-O-C} is the average Cu−O−C bond angle, θ_{Cu-O-H} is the average Cu−O−H bond angle, and θ_{C-O-H} is the average C−O−H bond angle. Since the C, Cu, O, and H atoms are able to form a pyramidal shape, eq 3 indicates that the pyramid solid angle at the O atom corner can be described. Though eq 3 is not an equation to calculate the real solid angle at O atom, Ω_O still can represent the angular relationship between

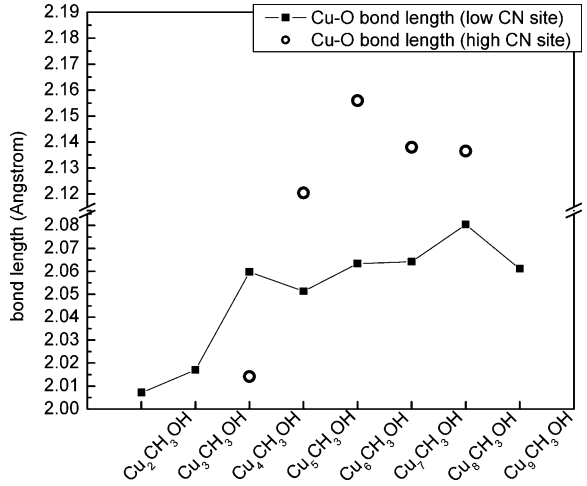

Figure 10. Cu−O bond lengths in the copper clusters. The solid squares represent the bond length for collision at a low CN site, and hollow circles indicate the bond length for collision at a high CN site.

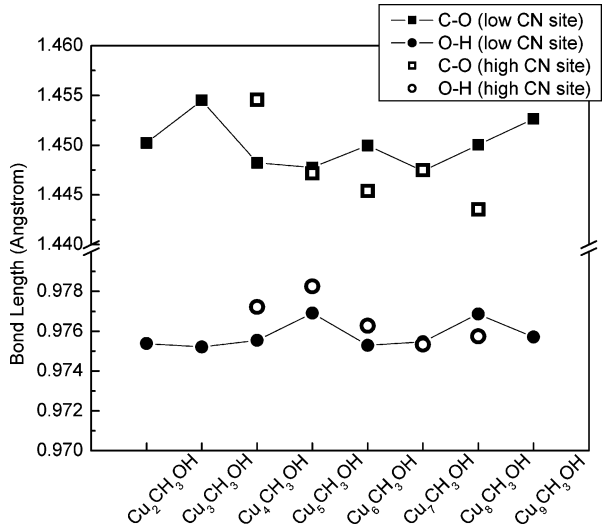

Figure 11. C−O bond length and O−H bond length in the copper clusters. The solid squares and circles represent the bond lengths for collision at low CN sites, and hollow squares and circles indicate the bond lengths for collision at high CN sites.

the O atom and its three neighbor atoms (Cu, C, and H). If Ω_O = zero, this means that the O, Cu, C, and H atoms are in the same plane. The larger Ω_O, the sharper the pyramid solid angle at the O atom corner.

In Figure 10, the Cu−O bond length is found to generally increase when the cluster size increases. Typically even-numbered clusters have longer Cu−O bond lengths. The three-stage trend in dimensionality with clusters size shown in bare copper clusters is not observed here. However, it is found that the Cu−O bond length is longer if the methanol molecule is adsorbed on the high CN site. The only exception is Cu_4CH_3OH, which has a shorter Cu−O bond length when the methanol molecule is adsorbed on a high CN site. This is most likely because the Cu_4 cluster changed its structure substantially following adsorption, as discussed above.

The resulting C−O bond lengths are shown in Figure 11. The C−O bond length trends are the opposite of the Cu−O bond length trend. For example, the high CN site Cu cluster−methanol compounds have a shorter C−O bond length and the lower CN site compounds have longer C−O bond lengths. The only exception is again Cu_4CH_3OH. This result indicates that

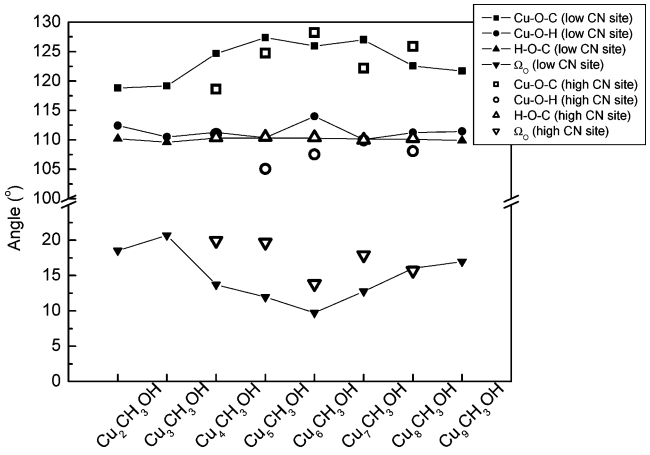

Figure 12. Bonding angles in Cu_nCH_3OH. The filled symbols represent the bonding angle for collision at low CN sites, and empty symbols indicate the bonding angle for collision at high CN sites.

the charge on the O atom is higher when the Cu−O bond length is shorter. From the bare copper cluster calculations discussed in the previous section, the low CN Cu site has higher charge than the high CN Cu site. The results imply that to adsorb a methanol molecule on a neutral copper cluster, there should be electron cloud transfer between the copper cluster and the methanol molecule. Higher electron cloud density provides more opportunity to achieve this transfer, which makes the low CN site most favorable for adsorption.

Comparing the C−O bond length of bare methanol and the adsorbed methanol molecule, the C−O bond length of adsorbed methanol is elongated when adsorbed at both the high CN site and the low CN site. The amount of elongation is approximately 0.02 Å (1.4%) at the low CN site and approximately 0.016 Å (1.1%) at the high CN site. This finding further confirms the analysis discussed above. In the isolated methanol molecule the C−O interaction is through σ-bonding, while when it is adsorbed on the copper cluster, part of the O electron clouds interact with the Cu atom and part of the Cu atom's electron cloud transfers to the O atom.[26,37] The net transfer leads the adsorbed Cu atom to have a slight positive charge and the O atom to have a slight negative charge, therefore stabilizing adsorption.

The results of O−H bond lengths are also provided in Figure 11. The O−H bond lengths are all slightly longer than the O−H bond length of an isolated methanol molecule. However there is no obvious trend between the high CN site and the low CN site. For Cu_4−Cu_6, the high CN site has a longer O−H bond length, and for Cu_7 and Cu_8, the low CN site has a longer bond length. From the electronic calculation of the bare methanol molecule, the bond order for O−H is 0.78 and for C−O is 0.46. Thus, since the O−H bond is stronger than the C−O bond, the influence of the electron cloud transfer between Cu and O does not affect the O−H bond to any significant degree.

Figure 12 illustrates the angular relationship around the O atom after the methanol molecule adsorbs to the Cu clusters. It is interesting that the C−O−H angle does not change much in the different adsorption cases and the angles are almost the same as in the case of the isolated methanol molecule (109.094°). In contrast, the Cu−O−H angle and Cu−O−C angle have more substantial variations. There is no clear trend that indicates that adsorption at a high CN site or a low CN site influences the Cu−O−C angle. However, the Cu−O−H angle typically is larger when methanol is adsorbed at a low CN site than at a high CN site. The pyramid solid angle at an O atom corner (Ω_O) also has larger variation, and typically the low CN site has a smaller Ω_O which indicates a flatter O−Cu−C−H plane.

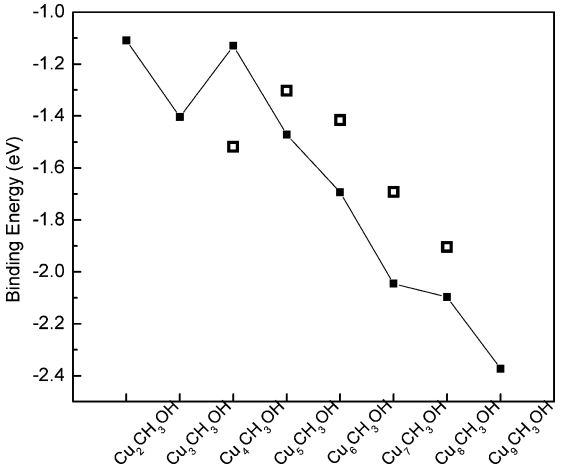

Figure 13. Binding energy in the copper clusters. The solid squares represent the binding energy for collision at low CN sites, and hollow squares indicate the binding energy for collision at high CN sites.

These angular relationships indicate how the methanol molecule adsorbs on the clusters. The small variation in C−O−H angle reveals that the covalent bonding nature (sp orbital hybridization) between the O−H and O−C is still strong after adsorption. The larger variations in the Cu−O−C angle and the Cu−O−H angle show that the bonding between Cu and O is not purely covalent but includes donation and back-donation of electrons. This illustrates how the Cu atom's 3d orbitals complicate the bond order that occurs as a result of adsorption.

The binding energy between the Cu clusters and methanol molecules are indicated in Figure 13. Here the binding energy is calculated through

$$\mathrm{BE} = E_{\mathrm{Cu_nCH_3OH}} - (E^{\mathrm{free}}_{\mathrm{CH_3OH}} + E^{\mathrm{free}}_{\mathrm{Cu_n}}) \qquad (4)$$

The results show that binding energies increase with increasing cluster size. This may conflict with our intuitive sense that with increasing cluster size the adsorption behavior should approach the behavior observed on Cu surfaces, which is purely physisorption.[11,29] This apparent contradiction is explained by the fact that, in the case of the largest cluster, Cu_9, considered in this study, the Cu atoms are far from a bulklike arrangement.

The results of binding energy also indicate that the adsorption site influences the binding energy. In particular, binding energy is higher when the methanol molecule is adsorbed on a low CN site and is lower when the methanol molecule is adsorbed on a high CN site. This result is consistent with our bond length results and accompanying analysis. The only exception is again Cu_4CH_3OH. As discussed above, this is because the structure of the Cu_4 cluster deforms significantly when methanol adsorbs on a low CN site. It becomes a Cu_3 structure attached to an extra Cu atom on one of its corner. Thus it is difficult to compare the result with the high CN site of the Cu_4 cluster.

At last it should be mentioned that the spin-polarized wave function with the GGA is also used in Cu_6CH_3OH and Cu_7CH_3OH to verify the result obtained by non-spin-polarized function in DFT−MD calculations. The equilibrium structures obtained by both methods are very similar, and the differences are within 1%. The results in binding energy also give the same trend, and the differences are within 7%. Thus it is believed that nonpolarized wave functions provide the most reliable results.

Conclusions

This study has analyzed the structure of small bare copper clusters and adsorption of methanol molecule on these clusters. It is found that the structural dimensionality of the bare copper clusters evolves with cluster size in average bond length, binding energy per bond, and bond order. The bond length increases with increasing structural dimensionality. The binding energy per bond and the bond order, however, decrease with increasing structural dimensionality. These results are explained by the electronic structures of the clusters. The population of 4s and 4p orbitals exhibit different trends in the two-dimensional and three-dimensional clusters.

It is also found that even numbered Cu clusters are more stable than odd numbered Cu clusters. The electron density distributions on bare Cu clusters contribute to a significant degree to methanol adsorption. Low CN sites have higher electron densities and provide more opportunity for electron cloud transfer between cluster Cu atoms and molecular O atoms, which makes them the most favorable adsorption sites. The complex structure of Cu_nCH_3OH compounds prove that the 3d orbital is involved in the interactions.

Acknowledgment. W.-D.H. and S.B.S. gratefully acknowledge the support of the National Science Foundation through Grant CHE-0200838, and M.I. and T.K. acknowledge the support of the Special Cluster Research Project of Genesis Research Institute, Inc.

References and Notes

(1) Parsons, R.; Vandernoot, T. *J. Electroanal. Chem.* **1988**, *257*, 9−45.
(2) Konopka, M.; Rousseau, R.; Stich, I.; Marx, D. *J. Am. Chem. Soc.* **2004**, *126*, 12103−12111.
(3) Shinn, N. D. *Surf. Sci.* **1992**, *278*, 157−165.
(4) Huberty, J. S.; Madix, R. J. *Surf. Sci.* **1996**, *360*, 144−156.
(5) Bare, S. R.; Stroscio, J. A.; Ho, W. *Surf. Sci.* **1985**, *150*, 399−418.
(6) Camplin, J. P.; McCash, E. M. *Surf. Sci.* **1996**, *360*, 229−241.
(7) Silva, S. L.; Lemor, R. M.; Leibsle, F. M. *Surf. Sci.* **1999**, *421*, 135−145.
(8) Sim, W. S.; Gardner, P.; King, D. A. *J. Phys. Chem.* **1995**, *99*, 16002−16010.
(9) Chen, J. J.; Jiang, Z. C.; Zhou, Y.; Chakraborty, B. R.; Winograd, N. *Surf. Sci.* **1995**, *328*, 248−262.
(10) Endo, M.; Matsumoto, T.; Kubota, J.; Domen, K.; Hirose, C. *Surf. Sci.* **1999**, *441*, L931−L937.
(11) Gomes, J. R. B.; Gomes, J. *Surf. Sci.* **2001**, *471*, 59−70.
(12) Gomes, J. R. B.; Gomes, J.; Illas, F. *J. Mol. Catal. A: Chem.* **2001**, *170*, 187−193.
(13) Jones, A. H.; Poulston, S.; Bennett, R. A.; Bowker, M. *Surf. Sci.* **1997**, *380*, 31−44.
(14) Greeley, J.; Mavrikakis, M. *J. Catal.* **2002**, *208*, 291−300.
(15) Greeley, J.; Mavrikakis, M. *J. Am. Chem. Soc.* **2002**, *124*, 7193−7201.
(16) Janssens, E.; Van Hoof, T.; Veldeman, N.; Neukermans, S.; Hou, M.; Lievens, P. *Int. J. Mass Spectrom.* **2006**, *252*, 38−46.
(17) Alayan, R.; Arnaud, L.; Broyer, M.; Cottancin, E.; Lerme, J.; Vialle, J. L.; Pellarin, M. *Phys. Rev. B* **2006**, *73*, 125444.
(18) Doppner, T.; Fennel, T.; Radcliffe, P.; Tiggesbaumker, J.; Meiwes-Broer, K. H. *Phys. Rev. A* **2006**, *73*, 031202.
(19) Keen, A. L.; Doster, M.; Han, H.; Johnson, S. A. *Chem. Commun. (Cambridge)* **2006**, 1221−1223.
(20) Mednikov, E. G.; Wittayakun, J.; Dahl, L. F. *J. Cluster Sci.* **2005**, *16*, 429−454.
(21) Jaque, P.; Toro-Labbe, A. *J. Chem. Phys.* **2002**, *117*, 3208−3218.
(22) Jug, K.; Zimmermann, B.; Calaminici, P.; Koster, A. M. *J. Chem. Phys.* **2002**, *116*, 4497−4507.
(23) Guvelioglu, G. H.; Ma, P. P.; He, X. Y.; Forrey, R. C.; Cheng, H. S. *Phys. Rev. B* **2006**, *73*, 155436.
(24) Wang, J.; Han, J. G. *J. Phys. Chem.* B **2006**, *110*, 7820−7827.
(25) Aguilera-Granja, F.; Montejano-Carrizalez, J. M.; Guirado-Lopez, R. A. *Phys. Rev. B* **2006**, *73*, 115422.
(26) Poater, A.; Duran, M.; Jaque, P.; Toro-Labbe, A. *J. Phys. Chem. B* **2006**, *110*, 6526−6536.
(27) Ichihashi, M.; Hanmura, T.; Yadav, R. T.; Kondow, T. *J. Phys. Chem. A* **2000**, *104*, 11885−11890.
(28) Ichihashi, M.; Corbett, C. A.; Hanmura, T.; Lisy, J. M.; Kondow, T. *J. Phys. Chem. A* **2005**, *109*, 7872−7880.

(29) Wang, G. C.; Zhou, Y. H.; Morikawa, Y.; Nakamura, J.; Cai, Z. S.; Zhao, X. Z. *J. Phys. Chem. B* **2005**, *109*, 12431−12442.
(30) Majumder, C.; Kulshreshtha, S. K. *Phys. Rev. B* **2006**, *73*, 155427.
(31) Rajesh, C.; Majumder, C.; Rajan, M. G. R.; Kulshreshtha, S. K. *Phys. Rev. B* **2005**, *72*, 235411.
(32) Deheer, W. A. *Rev. Mod. Phys.* **1993**, *65*, 611−676.
(33) Brack, M. *Rev. Mod. Phys.* **1993**, *65*, 677−732.
(34) Spasov, V. A.; Lee, T. H.; Ervin, K. M. *J. Chem. Phys.* **2000**, *112*, 1713−1720.
(35) Rao, B. K.; Jena, P. *Phys. Rev. Lett.* **1996**, *76*, 2878−2881.
(36) Yadav, R. T.; Ichihashi, M.; Kondow, T. *J. Phys. Chem. A* **2004**, *108*, 7188−7192.
(37) Rousseau, R.; Marx, D. *J. Chem. Phys.* **2000**, *112*, 761−769.
(38) Pasquarello, A.; Laasonen, K.; Car, R.; Lee, C. Y.; Vanderbilt, D. *Phys. Rev. Lett.* **1992**, *69*, 1982−1985.
(39) Payne, M. C.; Teter, M. P.; Allan, D. C.; Arias, T. A.; Joannopoulos, J. D. *Rev. Mod. Phys.* **1992**, *64*, 1045−1097.
(40) Arias, T. A.; Payne, M. C.; Joannopoulos, J. D. *Phys. Rev. Lett.* **1992**, *69*, 1077−1080.
(41) Segall, M. D.; Lindan, P. J. D.; Probert, M. J.; Pickard, C. J.; Hasnip, P. J.; Clark, S. J.; Payne, M. C. *J. Phys.-Condens. Matter* **2002**, *14*, 2717−2744.
(42) Payne, M. C.; Joannopoulos, J. D.; Allan, D. C.; Teter, M. P.; Vanderbilt, D. H. *Phys. Rev. Lett.* **1986**, *56*, 2656−2656.
(43) Laasonen, K.; Car, R.; Lee, C.; Vanderbilt, D. *Phys. Rev. B* **1991**, *43*, 6796−6799.
(44) White, J. A.; Bird, D. M. *Phys. Rev. B* **1994**, *50*, 4954−4957.
(45) Irle, S.; Zheng, G. S.; Elstner, M.; Morokuma, K. *Nano Lett.* **2003**, *3*, 1657−1664.
(46) Irle, S.; Zheng, G. S.; Elstner, M.; Morokuma, K. *Nano Lett.* **2003**, *3*, 465−470.
(47) Westergren, J.; Gronbeck, H.; Kim, S. G.; Tomanek, D. *J. Chem. Phys.* **1997**, *107*, 3071−3079.
(48) Gronbeck, H.; Tomanek, D.; Kim, S. G.; Rosen, A. *Chem. Phys. Lett.* **1997**, *264*, 39−43.
(49) Balbuena, P. B.; Derosa, P. A.; Seminario, J. M. *J. Phys. Chem. B* **1999**, *103*, 2830−2840.
(50) Jug, K.; Zimmermann, B.; Koster, A. M. *Int. J. Quantum Chem.* **2002**, *90*, 594−602.
(51) Narasimhan, S.; de Gironcoli, S. *Phys. Rev. B* **2002**, *65*, 064302.
(52) Lopez, N.; Norskov, J. K. *J. Am. Chem. Soc.* **2002**, *124*, 11262−11263.
(53) Ingolfsson, O.; Busolt, U.; Sugawara, K. *J. Chem. Phys.* **2000**, *112*, 4613−4620.
(54) Mulliken, R. S. *J. Chem. Phys.* **1955**, *23*, 1833−1840.